

Device physics of perovskite light-emitting diodes

Cite as: Appl. Phys. Rev. **11**, 041418 (2024); doi: [10.1063/5.0228117](https://doi.org/10.1063/5.0228117)

Submitted: 11 July 2024 · Accepted: 11 October 2024 ·

Published Online: 6 November 2024








View Online



Export Citation



CrossMark

Yuqi Sun,¹  Si Chen,¹  Jun-Yu Huang,^{1,2}  Yuh-Renn Wu,²  and Neil C. Greenham^{1,a)} 

AFFILIATIONS

¹Cavendish Laboratory, University of Cambridge, J.J. Thomson Avenue, Cambridge CB3 0HE, United Kingdom

²Graduate Institute of Photonics and Optoelectronics, National Taiwan University, Taipei 10617, Taiwan

^{a)}Author to whom correspondence should be addressed: ncg11@cam.ac.uk

ABSTRACT

Perovskite light-emitting diodes (LEDs) have emerged as a potential solution-processible technology that can offer efficient light emission with high color purity. Here, we explore the device physics of perovskite LEDs using simple analytical and drift-diffusion modeling, aiming to understand how the distribution of electric field, carrier densities, and recombination in these devices differs from those assumed in other technologies such as organic LEDs. High barriers to electron and hole extraction are responsible for the efficient recombination and lead to sharp build-up of electrons and holes close to the electron- and hole-blocking barriers, respectively. Despite the strongly varying carrier distributions, bimolecular recombination is surprisingly uniform throughout the device thickness, consistent with the assumption typically made in optical models. The current density is largely determined by injection from the metal electrodes, with a balance of electron and hole injection maintained by redistribution of electric field within the device by build-up of space charge.

© 2024 Author(s). All article content, except where otherwise noted, is licensed under a Creative Commons Attribution (CC BY) license (<https://creativecommons.org/licenses/by/4.0/>). <https://doi.org/10.1063/5.0228117>

I. INTRODUCTION

III-V compound semiconductor LEDs (III-V LEDs) and organic LEDs (OLEDs) have been commercialized as the mainstream LED technologies. Perovskite LEDs (PeLEDs) have recently emerged as a promising technology for next-generation light emitters due to their high efficiency, high color purity, and solution processibility.^{1–10} While materials and device engineering has led to significant improvement in the performance of PeLEDs, the underlying working principles behind their superb performance have not been extensively studied. To achieve further control over the performance of PeLEDs, it is important to investigate their mechanisms of device operation.

As III-V, organic, and perovskite LEDs each have distinct materials properties and device structures, their working principles can differ.^{1,11–18} In III-V LEDs, the emission is typically confined to a series of ultrathin quantum wells, whereas in OLEDs and PeLEDs, the emissive layer is generally thicker and surrounded by charge-transport layers designed to assist the injection and transport of electrons and holes from the electrodes. Although the structure of PeLEDs resembles that of OLEDs, the emissive layer generally has much higher and more balanced electron and hole mobilities. Hence, the device physics may differ significantly, and this will be particularly important in PeLEDs with thicker emissive layers that are becoming increasingly popular.

Electrical simulation of semiconductor devices is useful to investigate the physical processes that control their operation. Drift-diffusion models coupled with the Poisson equation are widely used to simulate LEDs to understand the behavior of charge carriers in the devices.^{19–27} In OLED models, the recombination is often found to occur close to the interface.¹⁹ The high charge densities also lead to strong space charge effects where the electric field varies significantly within the device. However, we find that PeLEDs show a more symmetric charge carrier distribution, with more uniform distributions of electric field and radiative recombination in the emissive layer. In this work, we focus on PeLEDs and understand how the injection, transport, and recombination processes affect device behavior, including the current-voltage characteristics, efficiency, and recombination profile, the latter being important for understanding optical outcoupling. We aim to answer the following questions related to the device physics of PeLEDs:

- (1) What controls the internal quantum efficiency?
- (2) Where is the emission zone?
- (3) What determines the current-voltage characteristics?

The physics of perovskite devices is significantly complicated by the presence of mobile ions. These relatively slowly moving ions can

lead to hysteresis in current–voltage curves and will tend to accumulate close to interfaces in the steady state. Recent drift-diffusion modeling of PeLEDs including ions has been reported by Sowmeh *et al.*, focusing on explaining time-dependent behavior.²⁷ We will initially neglect ions in order to provide a simple qualitative picture in the steady state that can motivate device design. Comparison with the more complex simulations including ions reveals that many of the key features of our simple model are retained in the presence of a steady-state ion distribution.

II. WORKING PRINCIPLES OF PEROVSKITE LIGHT-EMITTING DIODES

The factors determining the device behavior of PeLEDs relate to the bulk properties of each layer and also barriers at interfaces. Here, we consider a model of a typical PeLED with structure anode/HTL (40 nm)/EML (25 nm)/ETL (40 nm)/cathode (Fig. 1). HTL, EML, and ETL represent hole transport layer, emissive layer, and electron transport layer, respectively. This structure is an archetypical model similar to some typical FAPbI₃ PeLEDs in the literature.^{4,7} Note that we use this device model as a demonstration to describe a general picture of the working mechanisms of PeLEDs, rather than to fit specific device data. In Fig. 1, we define the energy offsets in the conduction (ΔE_c) and valence bands (ΔE_v) at each of the relevant interfaces in the device.

The key material parameters of each layer are shown in Table I. These parameters were selected to represent a typical PeLED model, with the aim of describing a general picture of the operation mechanisms. The energy levels of the EML are based on data from a previous report.²⁸ The energy levels of the HTL and ETL are chosen initially assuming that the transport layers have a large bandgap preventing carrier leakage and that all barriers are symmetrical for electrons and holes. Other parameters of the HTL and ETL, such as dielectric constant, mobilities, and recombination rate constants, are chosen to represent general organic transport layers used in PeLEDs. The reported values of dielectric constant and mobility of perovskites vary with different forms and preparations.^{28–32} We choose the parameters for the EML considering that perovskites typically have higher dielectric constant and mobility than organic transport layers. Carrier lifetime and recombination rates of the EML are extracted from the carrier density dynamics measured by ultrafast transient absorption spectroscopy.⁷ We use a one-dimensional drift-diffusion charge control (1D-DDCC) numerical solver

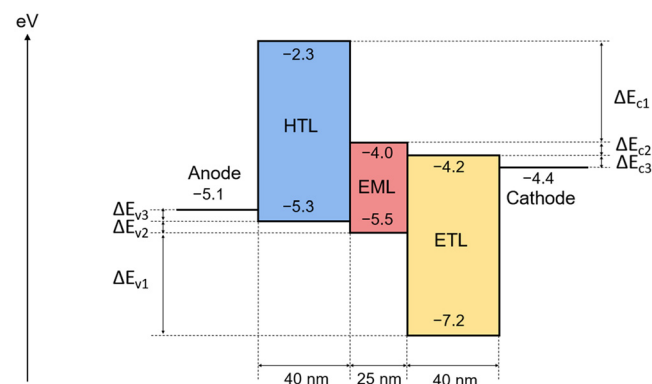


FIG. 1. Energy level diagram of an archetypical PeLED model.

TABLE I. Parameters for the artificial materials of the device models for PeLEDs.

Layer	HTL	EML	ETL
Thickness (nm)	40	25	40
Dielectric constant	3	10	3
μ_e / μ_h (cm ² /V s)	$10^{-3}/10^{-3}$	0.2/3.5	$10^{-3}/10^{-3}$
Conduction band energy (eV)	2.3	4.0	4.2
Valence band energy (eV)	5.3	5.5	7.2
Carrier lifetime (s)	-	1.6×10^{-7}	-
Radiative recombination rate constant (cm ³ s ⁻¹)	1×10^{-11}	8.7×10^{-11}	1×10^{-11}
Auger recombination rate constant (cm ⁶ s ⁻¹)	-	1.4×10^{-29}	-

to investigate this PeLED model.^{33,34} For simplicity, we have not included ions in this model. Also, all mobilities are taken to be independent of electric field and carrier density. The justification for these assumptions and the resulting limitations will be discussed later.

A. Internal quantum efficiency

The internal quantum efficiency (IQE) represents the efficiency of photon generation in the EML. IQE is defined as the ratio of the number of radiative recombination events to the number of electrons flowing through the external circuit, which is determined by the electrical efficiency (η_{el}) and the radiative efficiency (η_{rad}). IQE is given by

$$IQE = \eta_{el} \times \eta_{rad}. \quad (1)$$

Here, η_{el} is defined as the ratio of the total number of recombination events occurring in the EML to the number of electrons flowing through the external circuit. Electrical loss, or current leakage (corresponding to $\eta_{el} < 1$), occurs when charge carriers pass through the EML and escape without recombination. Typically, carriers are confined within the EML by the extraction barriers, which are much larger than the thermal energy at a room temperature (kT). η_{rad} is defined as the ratio of radiative recombination events to the total recombination events in the EML. The loss of IQE discussed below may arise from electrical loss or non-radiative recombination.

In the baseline PeLED model, the electron extraction barrier ΔE_{c1} and hole extraction barrier ΔE_{v1} are both 1.7 eV, which is large enough to prevent electrical loss via current leakage. Hence, η_{el} must be 100%. To understand the effect of the height of the extraction barriers on the device behavior, we simulated devices where the extraction barriers are tuned from 1.7 eV to 0.1 eV. The current density in the device is insensitive to the extraction barriers [Fig. 2(a)], while η_{el} depends on the height of the extraction barriers [Fig. 2(b)]. η_{el} remains close to 100% when the extraction barrier ΔE_{c1} is reduced from 1.7 eV to 0.3 eV. However, at high voltages, η_{el} drops dramatically when ΔE_{c1} is reduced to 0.2 eV and further drops to 20% if ΔE_{c1} is reduced to 0.1 eV. Similar results also apply to the hole extraction barrier ΔE_{v1} (supplementary Fig. 1).

To investigate the electrical loss, we simulated overflow current in the devices [Fig. 2(c)], which is the leakage current flowing through the device without recombination. In the control device, the overflow current is nearly zero. When the extraction barrier is reduced from 0.3 eV to 0.1 eV, the overflow current increases by orders of magnitude

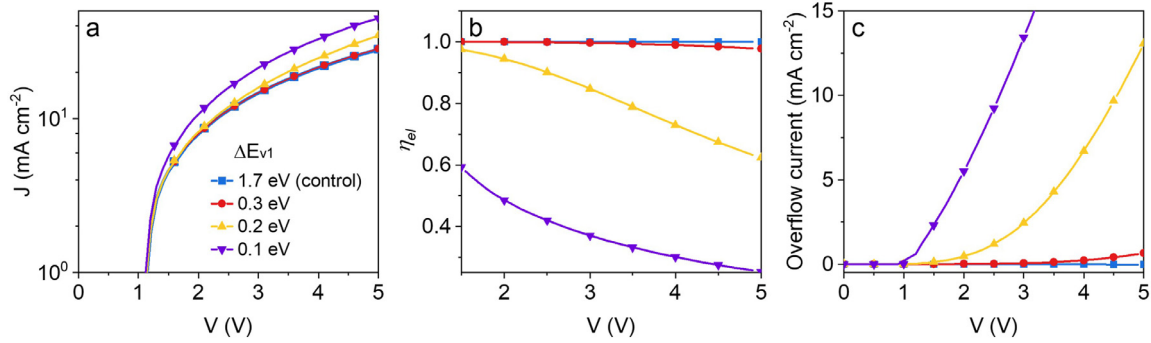


FIG. 2. Current density vs voltage characteristics (a); electrical efficiency η_{el} vs voltage characteristics (b); and overflow current vs voltage characteristics (c) for various electron extraction barriers ΔE_{c1} .

and therefore the electrical efficiency drops dramatically with small extraction barriers. This implies that η_{el} is controlled by the extraction barriers, which confine the carriers within the EML. In this model, the difference of the bandgaps between the EML (~ 1.5 eV) and the transport layers (~ 3.0 eV) is large and the extraction barriers are large enough to prevent carrier leakage. This is likely to be realistic for infrared- and red-emitting PeLEDs. However, green- and blue-emitting perovskites typically have a deep valence band (~ 6.1 eV) as a consequence of their high bandgap (> 2.4 eV).^{35–37} These devices typically use TPBi as an ETL, which has a HOMO level of ~ 6.2 eV.^{35,36} The hole extraction barrier is thus very small (~ 0.1 eV), which will be insufficient to confine the charge carriers within the EML (supplementary Fig. 2). Electrical loss may therefore be a major quantum efficiency loss in green and blue devices.

As long as the electrical efficiency η_{el} is 100%, IQE is only dependent on the radiative efficiency η_{rad} , which is a competition between radiative and non-radiative recombination (Shockley–Read–Hall (SRH) and Auger recombination).^{38,39} As shown in Fig. 3, the peak IQE is strongly dependent on the monomolecular carrier lifetime, which is determined by the SRH recombination rate. The peak IQE increases with a longer carrier lifetime, while IQE drops significantly with reduced carrier lifetime as the efficiency loss is primarily due to SRH recombination at low current densities. As current densities rise,

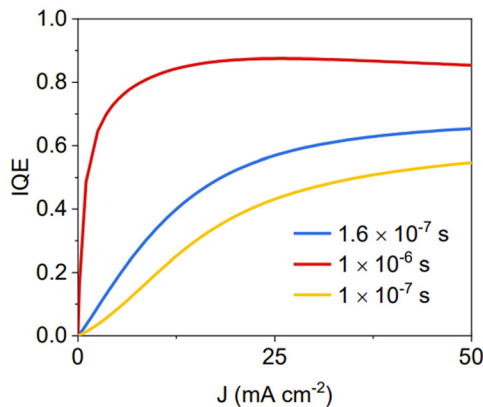


FIG. 3. IQE vs current density in the control device for various carrier lifetimes.

bimolecular recombination becomes more significant, leading to an increase in IQE. However, Auger recombination also increases as current densities rise, resulting in a decrease in radiative efficiency at high current densities (supplementary Fig. 3).

B. Emission profile

The profile of the emission zone in the EML is important to understand the device operation and to design the device structure (e.g., to optimize optical outcoupling). In this PeLED model, bimolecular recombination is considered as the radiative emission mechanism. From numerical simulation results, although the carrier density within the EML layer varies by orders of magnitude [Fig. 4(a)], the radiative recombination profile is nearly homogenous across the EML [Fig. 4(b)]. As there is more than an order of magnitude difference between the electron and hole mobilities of the EML (Table I), the difference between the electron and hole diffusion coefficients is also more than an order of magnitude according to the Einstein relation. However, we notice that densities of electrons and holes decay exponentially in the EML with nearly the same decay length of 3.4 nm [Fig. 4(a)]. This indicates that this characteristic decay length is independent of material properties such as diffusion coefficient. The fact that the carrier densities are so symmetric (despite the asymmetry in transport properties) and the recombination profile is so uniform (despite the very non-uniform carrier densities) may be a surprise to those familiar with OLED models and is worthy of further explanation.

Before analyzing the drift-diffusion simulations further, we consider a simple analytical model for the same device structure in the presence of a constant electric field E . If we initially consider electrons confined by a large barrier at $x = 0$ and in the absence of recombination, the drift and diffusion currents must balance to zero, giving

$$J_n = J_{drift-n} + J_{diff-n} = qn\mu_n E + qD_n \frac{dn}{dx} = 0. \quad (2)$$

Applying the Einstein relationship $D = \mu \frac{kT}{q}$, the solution is

$$n = n_0 e^{-\frac{x}{L_t}}, \quad (3)$$

where

$$L_t = \frac{kT}{qE}. \quad (4)$$

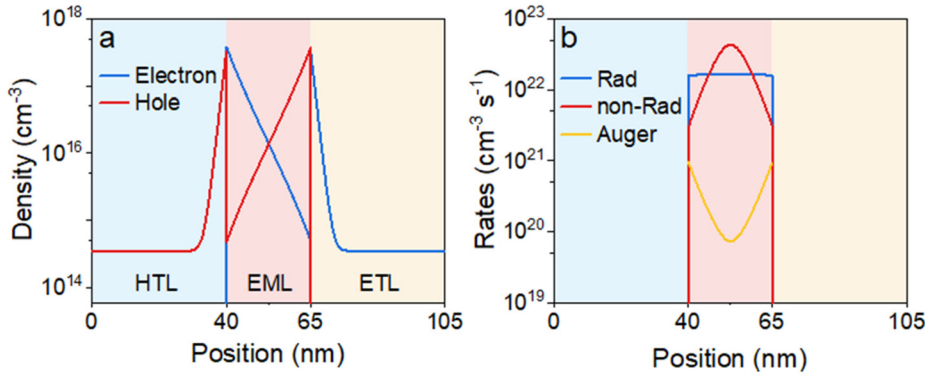


FIG. 4. Simulated distribution of carrier densities (a) and recombination rates (b) of the control device.

Similarly, for holes confined by a barrier at $x = a$, the carrier density is

$$p = p_0 e^{-\frac{a-x}{L_t}}. \quad (5)$$

We note that the decay lengths for electrons and holes are dependent only on the electric field and not on transport properties.

We now superimpose these electron and hole densities as shown in Fig. 5 and introduce bimolecular recombination under the assumption that this does not significantly alter the carrier densities. We further assume that the electric field is constant across the EML. The bimolecular recombination rate is given by

$$R = Bnp = Bn_0p_0 e^{-\left(\frac{x}{L_t}\right)}. \quad (6)$$

Hence, this simple model predicts completely uniform recombination across the EML. Comparing with the drift-diffusion simulations, we see behavior that is remarkably consistent with the simple model. The electric field within the EML is relatively constant (implying that space charge effects are weak), justifying this assumption in the simple model. The electron and hole densities decay exponentially, and the radiative recombination is uniform.

For the device operating at 3 V, the average electric field from Fig. 6(a) gives a value of $L_t = 3.7$ nm, close to the decay length of 3.4 nm

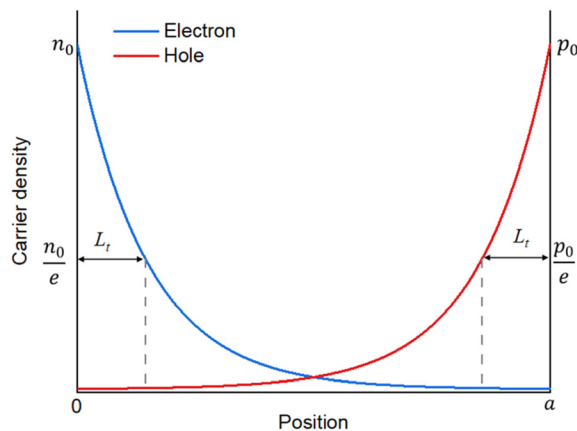


FIG. 5. Carrier density vs position within the EML in a hypothetical device without recombination. L_t is the characteristic decay length over which the charge carrier densities decay to $1/e$ of their initial value.

for both the electron and hole densities in the numerical model [Fig. 4(a)]. This close correspondence implies that the assumption that the recombination does not significantly influence the carrier density distributions is a good one. This can be rationalized by understanding that, when the device is operating (with a total current equal to the recombination current), this current is much smaller (by about two orders of magnitude) than the individual drift and diffusion currents for electrons and holes [Figs. 6(b) and (c)]. The carrier densities determined by the balance of drift and diffusion currents in the simple model are therefore not much changed when recombination and net current flow are introduced, since the drift and diffusion currents, although not perfectly balanced, are still almost balanced.

C. Current-voltage characteristics

The current-voltage characteristics can be determined by injection barriers or bulk effects such as the build-up of space charge. For materials with low mobility, such as polymers, space charge effects can be the dominant factor limiting the current flowing in a device.⁴⁰ Under ideal conditions for a single-carrier current, the space-charge-limited current is determined by the Mott-Gurney law,

$$J_{\text{SCL}} = \frac{9}{8} \epsilon \mu \frac{V^2}{d^3}, \quad (7)$$

where ϵ is the permittivity of the material, V is the applied voltage, and d represents the sample thickness. If the current is space-charge-limited, the current at constant voltage scales as d^{-3} , where d is the layer thickness. As shown in Fig. 7(a), the current density in the simulations is independent of the thickness of the EML. The current does depend on the thickness of the HTL or ETL [Figs. 7(b) and 7(c)], but these changes are much smaller than those predicted by the Mott-Gurney law. This indicates that bulk space-charge effects are not the dominant factor contributing to the current-voltage characteristics in this model.

We further examine whether the injection barriers limit the current in the device. As shown in Figs. 8(a) and 8(b), the electron injection barrier ΔE_{c2} from the ETL to the EML has a minor effect on current density. However, small changes of the electron injection barrier ΔE_{c3} from the cathode to the ETL can cause change of orders of magnitude in the current density. Similar results also apply to the hole injection barriers (supplementary Fig. 4). Thus, we consider that the injection barriers from the electrodes to the ETL or HTL limit the current-voltage characteristics in this device.

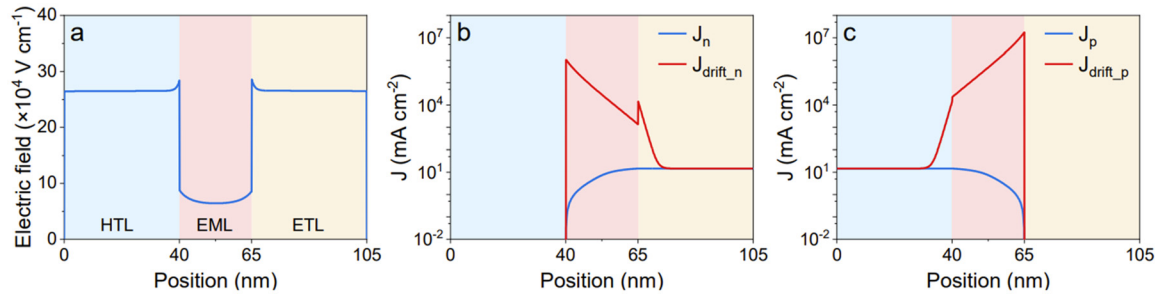


FIG. 6. Simulation of the electric field distribution in the device at 3 V (a), the total electron current and the electron drift current in the device at 3 V (b), and the total hole current and the hole drift current in the device at 3 V (c). For both electrons and holes, the diffusion current is the total current minus the drift current, and hence is almost equal and opposite to the drift current shown.

At an interface, if the device is close to thermal equilibrium (i.e., if the total current is small compared with the injected and reverse currents across the interface), the electron concentrations n_1 and n_2 on either side of an interface with energy barrier ΔE_c are related by Boltzmann statistics,

$$n_1 = n_2 e^{-\frac{\Delta E_c}{kT}}, \quad (8)$$

assuming identical densities of states. If we increase the injection barrier ΔE_{c2} at the ETL/EML interface, the electron density in the EML can be maintained at the same level by increasing the electron density on the ETL side of the interface [as seen in the drift-diffusion simulations in Figs. 8(c) and 8(e)]. Furthermore, the total accumulated charge is not sufficient to significantly influence the electric field distribution [Figs. 8(f) and 8(h)]. Therefore, the changes in ΔE_{c2} have a minimal impact on the current density within the EML.

The situation is different for the cathode/ETL interface, where increasing the injection barrier ΔE_{c3} leads to significantly reduced electron density in the ETL and hence in the EML [Figs. 8(i) and 8(k)]. As the electron density in the metal cathode is fixed, the electron density in the ETL depends directly on the injection barrier at the cathode/ETL interface, as described close to thermal equilibrium by Boltzmann statistics [Eq. (8)]. This means that an increase in the injection barrier results in a decrease in the electron density in the ETL, and vice versa. Given that the distribution of charge carriers changes significantly with the barrier, the electric field distribution also varies, as shown in Figs. 8(l) and 8(n). Thus, the total current density in the device is controlled by the injection barriers from the electrodes to the HTL or ETL.

We see that the current density in the device changes by orders of magnitude when we tune the electron injection barrier ΔE_{c3} , but we find that the electrical efficiency η_{el} remains unity as the extraction barrier is large enough to prevent current leakage as we discussed before. We have already seen how the electron current is controlled by ΔE_{c3} , but to maintain unity η_{el} , the hole current must change by the same amount, despite the fact that the hole injection barrier has not been changed (supplementary Fig. 5). To understand the mechanism that balances the electron and hole currents at their respective injecting electrodes, we examine the electric field distribution across the device. In the symmetrical situation (the control device), the electric fields in the HTL and ETL are nearly equal [Fig. 8(l)]. However, if the electron injection barrier ΔE_{c3} is reduced, less electric field is present in the ETL and more electric field builds up in the HTL to balance the current [Fig. 8(m)]. On the other hand, if ΔE_{c3} increases, more electric field builds up in the ETL and less electric field is present in the HTL [Fig. 8(n)]. If the injection barrier is changed on one side, the electric field across the entire device redistributes (due to space charge at interfaces and within the bulk of the device) to balance the electron injection current and hole injection current. Due to the extraction barriers, electrons and holes are confined within the EML for recombination, so the electrical efficiency is still 100%.

III. LIMITATIONS AND OUTLOOK

In this work, we have made some assumptions for simplicity to discuss the general device physics of PeLEDs. The justification and limitations of these assumptions are discussed as follows:

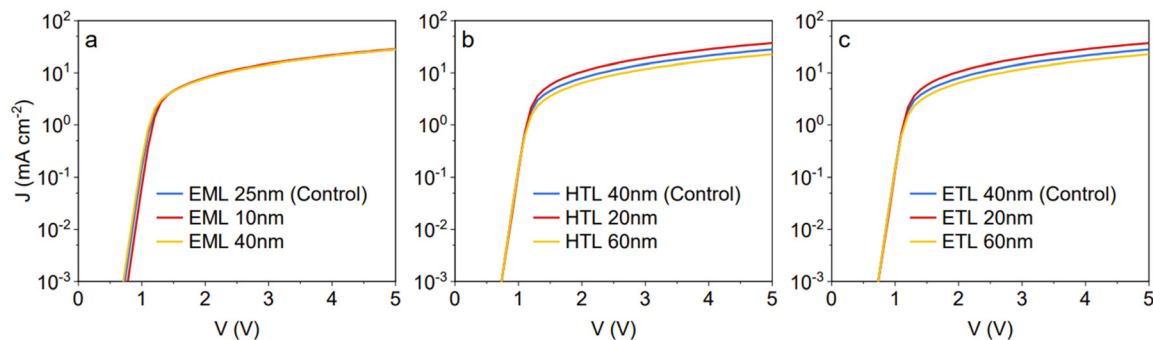


FIG. 7. Current density vs voltage characteristics of various thicknesses of the EML (a), the HTL (b), and the ETL (c).

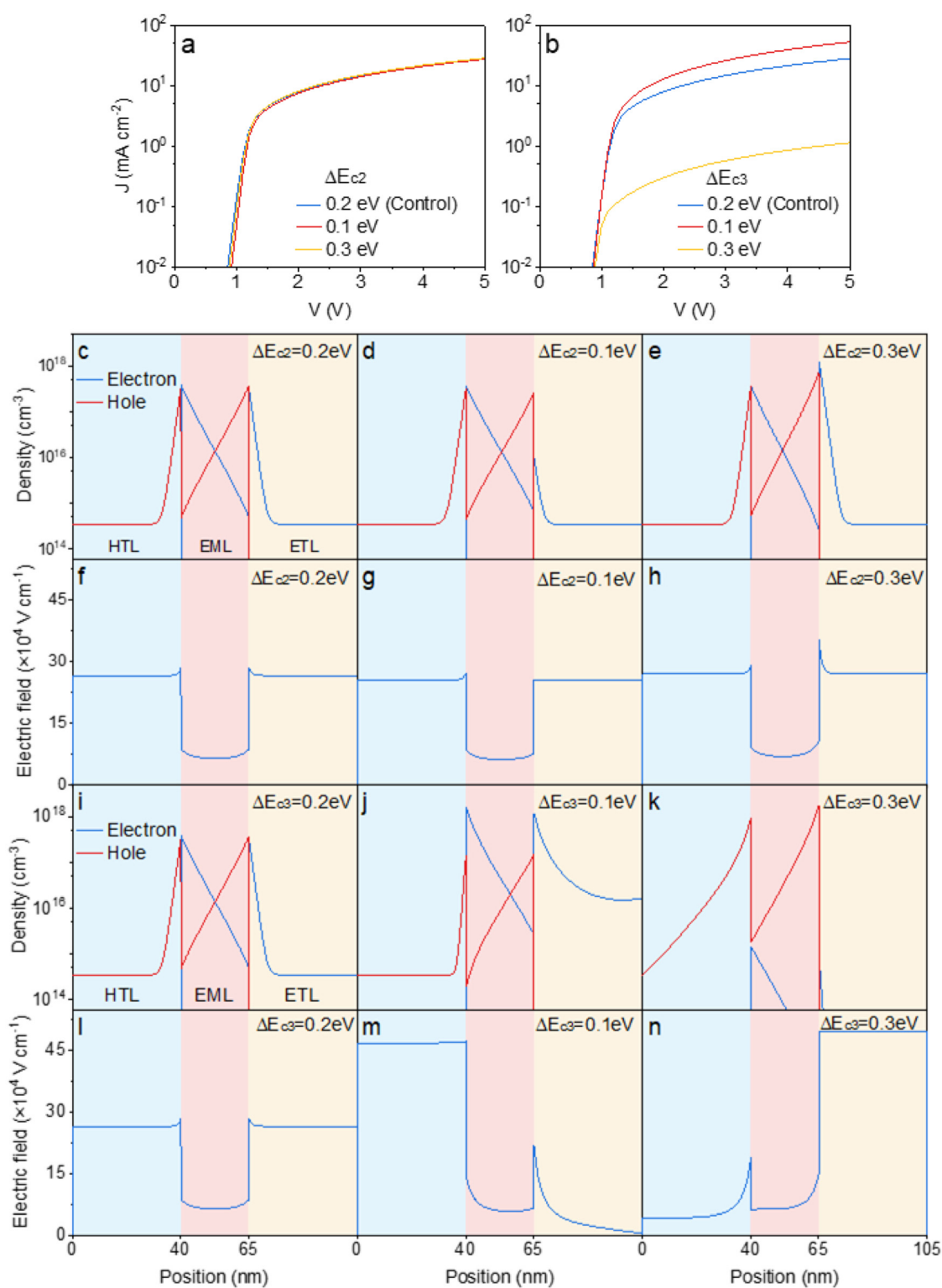


FIG. 8. Current density vs voltage characteristics for various injection barriers ΔE_{c2} (a) and ΔE_{c3} (b). Distribution of charge carriers (c–e) and electric fields (f–h) for various injection barriers ΔE_{c2} . Distribution of charge carriers (i–k) and electric fields (l–n) for various ΔE_{c3} (i–n).

In this model, we do not include the effect of ion migration, a well-known issue in perovskite materials.^{33,34} Although hysteresis in perovskite devices can be reduced by defect passivation and interfacial engineering,^{41–43} ion migration can still play an important role.⁴⁴ Mobile ions can accumulate at interfaces and facilitate charge injection.^{45,46} Also, the accumulation of ions at interfaces can screen the electric field within the perovskite layer.^{44,47} Such a reduction in the field would lead to a longer carrier decay length, but the recombination profile would still be flat except perhaps very close to the edges of the EML. Modeling the effects of ions is complex due to the different time-scales involved and due to the difficulties in accurately determining the ionic species present, their concentrations, and their mobilities and diffusion coefficients.^{34,48–51} Packages designed to simulate mixed ionic-electronic conducting devices are now available^{26,52–54} and have recently been applied to PeLEDs.²⁷ Those results show that, although the charge carrier densities vary by orders of magnitude, the product of the densities of electrons and holes (i.e., bimolecular recombination) remains uniform in the steady state when ions are included.²⁷

We have also made simplifying assumptions about the transport layers in this work. Organic materials (e.g., PVK, TPBi, TFB, and poly-TPD) and inorganic materials (e.g., ZnO and SnO₂) are commonly used as transport layers in PeLEDs. In this perovskite model, the two transport layers are considered as organic materials and the barriers and mobilities of the transport layer are selected to be symmetrical. Also, we do not include tail states in the organic transport layers and assume that mobility is independent of electric field and carrier density. In organic semiconductors where the densities of states are known to be broadened by disorder, mobilities become dependent in general upon field and carrier density, and injection may also be influenced by the energetic disorder.^{55,56} Similar effects may pertain in inorganic materials such as ZnO where defect states lead to a complex landscape of energy states.^{57–59} These effects will be important to include in models that can quantitatively predict current–voltage curves in particular experimental systems, although the simplified approach we have used is sufficient to illustrate the key processes determining the device operation.

While we have focused on electrical, rather than optical simulations, knowledge of recombination zone profiles is crucial to accurately predict outcoupling efficiencies in optical simulations. Future combined electrical and optical simulations will be able to fully model the measured light output, including effects, such as photon recycling,^{60–63} that can be particularly helpful in achieving high external efficiencies.

IV. CONCLUSION

In this study, we have modeled the device characteristics of an archetypical PeLED structure. In this model, the extraction barriers prevent current leakage and control the total recombination efficiency. If the extraction barriers fail to trap carriers within the EML, current leakage can lead to significant electrical loss. Due to the presence of high extraction barriers preventing carriers escape, the total recombination efficiency is unity and the height of the extraction barriers does not limit the device behavior. The current–voltage characteristics in this model are not limited by bulk effects such as space charge. Also, the injection barriers from the transport layers to the EML have only small effects on the current. However, the current flowing in the device is sensitive to the injection barriers from electrodes to the organic transport layers.

Electron and hole concentrations in the EML decay from the extraction barrier with a characteristic length determined by the

electric field and insensitive to diffusion coefficients and recombination processes. Despite the strongly varying electron and hole densities, the bimolecular recombination profile is uniform across the EML. The resulting uniform emission profile may have important implications for the design of light outcoupling strategies.

SUPPLEMENTARY MATERIALS

See the [supplementary material](#) for the following: a one-dimensional drift-diffusion charge control (1D-DDCC) numerical solver used in this work to investigate this PeLED model; current density vs voltage characteristics (a), electrical efficiency η_{el} vs voltage characteristics (b), and overflow current (c) for various hole extraction barriers ΔE_{v1} (supplementary Fig. 1); energy diagram of PeLEDs with blue-, green-, and red-emitting layers (supplementary Fig. 2); recombination quantum efficiency vs current density in the control device (supplementary Fig. 3); current density vs voltage characteristics for various injection barriers ΔE_{v2} (a) and ΔE_{v3} (b); distribution of charge carriers (c–e) and electric fields (f–h) for various injection barriers ΔE_{v2} ; distribution of charge carriers (i–k) and electric fields (l–m) for various ΔE_{v3} (i–n) (supplementary Fig. 4); and electron and hole current across the device with the electron injection barrier ΔE_{c3} of 0.2 eV (control) (a), 0.1 eV (b), and 0.3 eV (c) (supplementary Fig. 5).

ACKNOWLEDGMENTS

This work was supported by the Engineering and Physical Sciences Research Council, UK, through Grant Nos. EP/V06164X/1 and EP/S030638/1. Y. S. acknowledges support from the China Scholarship Council and the Cambridge Trusts. S. C. acknowledges support from the Cambridge Trusts. J.-Y.H. acknowledges support from the Simons Foundation (Grant No. 601946). Y.-R. W. acknowledges support from the National Science and Technology Council, Taiwan, Grant No. NSTC 112-2221-E-002-215-MY3.

AUTHOR DECLARATIONS

Conflict of Interest

The authors have no conflicts to disclose.

Author Contributions

Yuqi Sun: Conceptualization (lead); Investigation (lead); Writing – original draft (lead). **Si Chen:** Investigation (supporting). **Jun-Yu Huang:** Methodology (equal); Software (equal). **Yuh-Renn Wu:** Software (equal). **Neil C. Greenham:** Conceptualization (supporting); Supervision (lead); Writing – review & editing (lead).

DATA AVAILABILITY

The data that support this study are available at <https://doi.org/10.17863/CAM.113159>.

REFERENCES

- ¹Z.-K. Tan, R. S. Moghaddam, M. L. Lai, P. Docampo, R. Higler, F. Deschler, M. Price, A. Sadhanala, L. M. Pazos, D. Credgington, F. Hanusch, T. Bein, H. J. Snaith, and R. H. Friend, “Bright light-emitting diodes based on organometal halide perovskite,” *Nat. Nanotech.* **9**(9), 687–692 (2014).
- ²B. Zhao, S. Bai, V. Kim, R. Lamboll, R. Shivanna, F. Auras, J. M. Richter, L. Yang, L. Dai, M. Alsari, X.-J. She, L. Liang, J. Zhang, S. Lilliu, P. Gao, H. J.

- Snaith, J. Wang, N. C. Greenham, R. H. Friend, and D. Di, "High-efficiency perovskite-polymer bulk heterostructure light-emitting diodes," *Nat. Photonics* **12**(12), 783–789 (2018).
- ³N. Wang, L. Cheng, R. Ge, S. Zhang, Y. Miao, W. Zou, C. Yi, Y. Sun, Y. Cao, R. Yang, Y. Wei, Q. Guo, Y. Ke, M. Yu, Y. Jin, Y. Liu, Q. Ding, D. Di, L. Yang, G. Xing, H. Tian, C. Jin, F. Gao, R. H. Friend, J. Wang, and W. Huang, "Perovskite light-emitting diodes based on solution-processed self-organized multiple quantum wells," *Nat. Photonics* **10**(11), 699–704 (2016).
- ⁴Y. Cao, N. Wang, H. Tian, J. Guo, Y. Wei, H. Chen, Y. Miao, W. Zou, K. Pan, Y. He, H. Cao, Y. Ke, M. Xu, Y. Wang, M. Yang, K. Du, Z. Fu, D. Kong, D. Dai, Y. Jin, G. Li, H. Li, Q. Peng, J. Wang, and W. Huang, "Perovskite light-emitting diodes based on spontaneously formed submicrometre-scale structures," *Nature* **562**(7726), 249–253 (2018).
- ⁵D. Ma, K. Lin, Y. Dong, H. Choubisa, A. H. Proppe, D. Wu, Y.-K. Wang, B. Chen, P. Li, J. Z. Fan, F. Yuan, A. Johnston, Y. Liu, Y. Kang, Z.-H. Lu, Z. Wei, and E. H. Sargent, "Distribution control enables efficient reduced-dimensional perovskite LEDs," *Nature* **599**(7886), 594–598 (2021).
- ⁶K. Lin, J. Xing, L. N. Quan, F. P. G. de Arquer, X. Gong, J. Lu, L. Xie, W. Zhao, D. Zhang, C. Yan, W. Li, X. Liu, Y. Lu, J. Kirman, E. H. Sargent, Q. Xiong, and Z. Wei, "Perovskite light-emitting diodes with external quantum efficiency exceeding 20 per cent," *Nature* **562**(7726), 245–248 (2018).
- ⁷Y. Sun, L. Ge, L. Dai, C. Cho, J. F. Orri, K. Ji, S. J. Zelewski, Y. Liu, A. J. Mirabelli, Y. Zhang, J.-Y. Huang, Y. Wang, K. Gong, M. C. Lai, L. Zhang, D. Yang, J. Lin, E. M. Tennyson, C. Ducati, S. D. Stranks, L.-S. Cui, and N. C. Greenham, "Bright and stable perovskite light-emitting diodes in the near-infrared range," *Nature* **615**(7954), 830–835 (2023).
- ⁸H. Cho, S.-H. Jeong, M.-H. Park, Y.-H. Kim, C. Wolf, C.-L. Lee, J. H. Heo, A. Sadhanala, N. Myoung, S. Yoo, S. H. Im, R. H. Friend, and T.-W. Lee, "Overcoming the electroluminescence efficiency limitations of perovskite light-emitting diodes," *Science* **350**(6265), 1222–1225 (2015).
- ⁹J. S. Kim, J.-M. Heo, G.-S. Park, S.-J. Woo, C. Cho, H. J. Yun, D.-H. Kim, J. Park, S.-C. Lee, S.-H. Park, E. Yoon, N. C. Greenham, and T.-W. Lee, "Ultra-bright, efficient and stable perovskite light-emitting diodes," *Nature* **611**(7937), 688–694 (2022).
- ¹⁰B. Zhao, Y. Lian, L. Cui, G. Divitini, G. Kusch, E. Ruggeri, F. Auras, W. Li, D. Yang, B. Zhu, R. A. Oliver, J. L. MacManus-Driscoll, S. D. Stranks, D. Di, and R. H. Friend, "Efficient light-emitting diodes from mixed-dimensional perovskites on a fluoride interface," *Nat. Electron.* **3**(11), 704–710 (2020).
- ¹¹S. Nakamura, T. Mukai, and M. Senoh, "Candela-class high-brightness InGaN/AlGaIn double-heterostructure blue-light-emitting diodes," *Appl. Phys. Lett.* **64**(13), 1687–1689 (1994).
- ¹²S. Nakamura, "III-V nitride based light-emitting devices," *Solid State Commun.* **102**(2–3), 237–248 (1997).
- ¹³J. Cho, E. F. Schubert, and J. K. Kim, "Efficiency droop in light-emitting diodes: Challenges and countermeasures," *Laser Photonics Rev.* **7**(3), 408–421 (2013).
- ¹⁴C. W. Tang and S. A. VanSlyke, "Organic electroluminescent diodes," *Appl. Phys. Lett.* **51**(12), 913–915 (1987).
- ¹⁵C. W. Tang, S. A. VanSlyke, and C. H. Chen, "Electroluminescence of doped organic thin films," *J. Appl. Phys.* **65**(9), 3610–3616 (1989).
- ¹⁶J. H. Burroughes, D. D. C. Bradley, A. R. Brown, R. N. Marks, K. Mackay, R. H. Friend, P. L. Burns, and A. B. Holmes, "Light-emitting diodes based on conjugated polymers," *Nature* **347**(6293), 539–541 (1990).
- ¹⁷N. C. Greenham, S. C. Moratti, D. D. C. Bradley, R. H. Friend, and A. B. Holmes, "Efficient light-emitting diodes based on polymers with high electron affinities," *Nature* **365**(6447), 628–630 (1993).
- ¹⁸N. C. Greenham and R. H. Friend, "Semiconductor device physics of conjugated polymers," *Solid State Phys.* **49**, 1–149 (1996).
- ¹⁹B. Ruhstaller, S. A. Carter, S. Barth, H. Riel, W. Riess, and J. C. Scott, "Transient and steady-state behavior of space charges in multilayer organic light-emitting diodes," *J. Appl. Phys.* **89**(8), 4575–4586 (2001).
- ²⁰B. Ruhstaller, T. Flatz, M. Moos, G. Sartoris, M. Kiy, T. Beierlein, R. Kern, C. Winnewisser, R. Pretot, N. Chebotareva, and P. Schaaf, "Optoelectronic OLED modeling for device optimization and analysis," *SID Symp. Dig. Tech. Pap.* **38**(1), 1686–1690 (2007).
- ²¹J. A. Barker, C. M. Ramsdale, and N. C. Greenham, "Modeling the current-voltage characteristics of bilayer polymer photovoltaic devices," *Phys. Rev. B* **67**(7), 075205 (2003).
- ²²K. Murata, S. Cinà, and N. C. Greenham, "Barriers to electron extraction in polymer light-emitting diodes," *Appl. Phys. Lett.* **79**(8), 1193–1195 (2001).
- ²³G. G. Malliaras and J. C. Scott, "Numerical simulations of the electrical characteristics and the efficiencies of single-layer organic light emitting diodes," *J. Appl. Phys.* **85**(10), 7426–7432 (1999).
- ²⁴J.-Y. Huang, Y.-W. Yang, W.-H. Hsu, E.-W. Chang, M.-H. Chen, and Y.-R. Wu, "Influences of dielectric constant and scan rate on hysteresis effect in perovskite solar cell with simulation and experimental analyses," *Sci. Rep.* **12**(1), 7927 (2022).
- ²⁵C. D. J. Blades and A. B. Walker, "Simulation of organic light-emitting diodes," *Synth. Met.* **111–112**, 335–340 (2000).
- ²⁶P. Calado, I. Gelmetti, B. Hilton, M. Ezzouzi, J. Nelson, and P. R. F. Barnes, "Driftfusion: An open source code for simulating ordered semiconductor devices with mixed ionic-electronic conducting materials in one dimension," *J. Comput. Electron.* **21**(4), 960–991 (2022).
- ²⁷P. F. Sowmeah, M. Zohorfazeli, and E. Yazdani, "Understanding the influence of cation and anion migration on perovskite light-emitting diodes via transient response," *Sci. Rep.* **13**(1), 15643 (2023).
- ²⁸X. Zhao and Z.-K. Tan, "Large-area near-infrared perovskite light-emitting diodes," *Nat. Photonics* **14**, 215 (2020).
- ²⁹G. E. Eperon, S. D. Stranks, C. Menelaou, M. B. Johnston, L. M. Herz, and H. J. Snaith, "Formamidinium lead trihalide: A broadly tunable perovskite for efficient planar heterojunction solar cells," *Energy Environ. Sci.* **7**(3), 982 (2014).
- ³⁰L. M. Herz, "Charge-carrier dynamics in organic-inorganic metal halide perovskites," *Annu. Rev. Phys. Chem.* **67**(1), 65–89 (2016).
- ³¹Q. Han, S. Bae, P. Sun, Y. Hsieh, Y. Yang, Y. S. Rim, H. Zhao, Q. Chen, W. Shi, G. Li, and Y. Yang, "Single crystal formamidinium lead iodide (FAPbI₃): Insight into the structural, optical, and electrical properties," *Adv. Mater.* **28**(11), 2253–2258 (2016).
- ³²S. D. Stranks, G. E. Eperon, G. Grancini, C. Menelaou, M. J. P. Alcocer, T. Leijtens, L. M. Herz, A. Petrozza, and H. J. Snaith, "Electron-hole diffusion lengths exceeding 1 micrometer in an organometal trihalide perovskite absorber," *Science* **342**(6156), 341–344 (2013).
- ³³Y. Yuan and J. Huang, "Ion migration in organometal trihalide perovskites and its impact on photovoltaic efficiency and stability," *Acc. Chem. Res.* **49**(2), 286–293 (2016).
- ³⁴C. Eames, J. M. Frost, P. R. F. Barnes, B. C. O'Regan, A. Walsh, and M. S. Islam, "Ionic transport in hybrid lead iodide perovskite solar cells," *Nat. Commun.* **6**(1), 7497 (2015).
- ³⁵Z. Li, Z. Chen, Y. Yang, Q. Xue, H.-L. Yip, and Y. Cao, "Modulation of recombination zone position for quasi-two-dimensional blue perovskite light-emitting diodes with efficiency exceeding 5%," *Nat. Commun.* **10**(1), 1027 (2019).
- ³⁶M. K. Gangishetty, S. Hou, Q. Quan, and D. N. Congreve, "Reducing architecture limitations for efficient blue perovskite light-emitting diodes," *Adv. Mater.* **30**(20), 1706226 (2018).
- ³⁷T. Chiba, Y. Hayashi, H. Ebe, K. Hoshi, J. Sato, S. Sato, Y.-J. Pu, S. Ohisa, and J. Kido, "Anion-exchange red perovskite quantum dots with ammonium iodine salts for highly efficient light-emitting devices," *Nat. Photonics* **12**(11), 681–687 (2018).
- ³⁸S. D. Stranks, R. L. Z. Hoye, D. Di, R. H. Friend, and F. Deschler, "The physics of light emission in halide perovskite devices," *Adv. Mater.* **31**, 1803336 (2019).
- ³⁹J. M. Richter, M. Abdi-Jalebi, A. Sadhanala, M. Tabachnyk, J. P. H. Rivett, L. M. Pazos-Outón, K. C. Gödel, M. Price, F. Deschler, and R. H. Friend, "Enhancing photoluminescence yields in lead halide perovskites by photon recycling and light out-coupling," *Nat. Commun.* **7**(1), 13941 (2016).
- ⁴⁰V. D. Mihailetschi, J. Wildeman, and P. W. M. Blom, "Space-charge limited photocurrent," *Phys. Rev. Lett.* **94**(12), 126602 (2005).
- ⁴¹H. Tan, A. Jain, O. Voznyy, X. Lan, F. P. G. de Arquer, J. Z. Fan, R. Quintero-Bermudez, M. Yuan, B. Zhang, Y. Zhao, F. Fan, P. Li, L. N. Quan, Y. Zhao, Z.-H. Lu, Z. Yang, S. Hoogland, and E. H. Sargent, "Efficient and stable solution-processed planar perovskite solar cells via contact passivation," *Science* **355**(6326), 722–726 (2017).
- ⁴²B. Guo, R. Lai, S. Jiang, L. Zhou, Z. Ren, Y. Lian, P. Li, X. Cao, S. Xing, Y. Wang, W. Li, C. Zou, M. Chen, Z. Hong, C. Li, B. Zhao, and D. Di, "Ultrastable near-infrared perovskite light-emitting diodes," *Nat. Photonics* **16**(9), 637–643 (2022).

- ⁴³J. Peng, Y. Wu, W. Ye, D. A. Jacobs, H. Shen, X. Fu, Y. Wan, T. Duong, N. Wu, C. Barugkin, H. T. Nguyen, D. Zhong, J. Li, T. Lu, Y. Liu, M. N. Lockrey, K. J. Weber, K. R. Catchpole, and T. P. White, "Interface passivation using ultrathin polymer–fullerene films for high-efficiency perovskite solar cells with negligible hysteresis," *Energy Environ. Sci.* **10**(8), 1792–1800 (2017).
- ⁴⁴P. Calado, A. M. Telford, D. Bryant, X. Li, J. Nelson, B. C. O'Regan, and P. R. F. Barnes, "Evidence for ion migration in hybrid perovskite solar cells with minimal hysteresis," *Nat. Commun.* **7**(1), 13831 (2016).
- ⁴⁵E. Bandiello, J. Ávila, L. Gil-Escrig, E. Tekelenburg, M. Sessolo, and H. J. Bolink, "Influence of mobile ions on the electroluminescence characteristics of methylammonium lead iodide perovskite diodes," *J. Mater. Chem. A* **4**(47), 18614–18620 (2016).
- ⁴⁶Q. Dong, J. Mendes, L. Lei, D. Seyitliyev, L. Zhu, S. He, K. Gundogdu, and F. So, "Understanding the role of ion migration in the operation of perovskite light-emitting diodes by transient measurements," *ACS Appl. Mater. Interfaces* **12**(43), 48845–48853 (2020).
- ⁴⁷R. A. Belisle, W. H. Nguyen, A. R. Bowring, P. Calado, X. Li, S. J. C. Irvine, M. D. McGehee, P. R. F. Barnes, and B. C. O'Regan, "Interpretation of inverted photocurrent transients in organic lead halide perovskite solar cells: Proof of the field screening by mobile ions and determination of the space charge layer widths," *Energy Environ. Sci.* **10**(1), 192–204 (2017).
- ⁴⁸A. Buin, R. Comin, J. Xu, A. H. Ip, and E. H. Sargent, "Halide-dependent electronic structure of organolead perovskite materials," *Chem. Mater.* **27**(12), 4405–4412 (2015).
- ⁴⁹D. A. Egger, L. Kronik, and A. M. Rappe, "Theory of hydrogen migration in organic-inorganic halide perovskites," *Angew. Chem. Int. Ed.* **54**(42), 12437–12441 (2015).
- ⁵⁰K. Domanski, B. Roose, T. Matsui, M. Saliba, S.-H. Turren-Cruz, J.-P. Correa-Baena, C. R. Carmona, G. Richardson, J. M. Foster, F. D. Angelis, J. M. Ball, A. Petrozza, N. Mine, M. K. Nazeeruddin, W. Tress, M. Grätzel, U. Steiner, A. Hagfeldt, and A. Abate, "Migration of cations induces reversible performance losses over day/night cycling in perovskite solar cells," *Energy Environ. Sci.* **10**(2), 604–613 (2017).
- ⁵¹L. Bertoluzzi, C. C. Boyd, N. Rolston, J. Xu, R. Prasanna, B. C. O'Regan, and M. D. McGehee, "Mobile ion concentration measurement and open-access band diagram simulation platform for halide perovskite solar cells," *Joule* **4**(1), 109–127 (2020).
- ⁵²J. M. Cave, N. E. Courtier, I. A. Blackburn, T. W. Jones, D. Ghosh, K. F. Anderson, L. Lin, A. A. Dijkhoff, G. J. Wilson, K. Feron, M. S. Islam, J. M. Foster, G. Richardson, and A. B. Walker, "Deducing transport properties of mobile vacancies from perovskite solar cell characteristics," *J. Appl. Phys.* **128**(18), 184501 (2020).
- ⁵³W. Clarke, L. J. Bennett, Y. Grudeva, J. M. Foster, G. Richardson, and N. E. Courtier, "IonMonger 2.0: Software for free, fast and versatile simulation of current, voltage and impedance response of planar perovskite solar cells," *J. Comput. Electron.* **22**(1), 364–382 (2022).
- ⁵⁴N. E. Courtier, J. M. Cave, J. M. Foster, A. B. Walker, and G. Richardson, "How transport layer properties affect perovskite solar cell performance: Insights from a coupled charge transport/ion migration model," *Energy Environ. Sci.* **12**(1), 396–409 (2019).
- ⁵⁵V. Coropceanu, J. Cornil, D. A. d S. Filho, Y. Olivier, R. Silbey, and J.-L. Brédas, "Charge transport in organic semiconductors," *Chem. Rev.* **107**(4), 926–952 (2007).
- ⁵⁶H. Bässler, "Charge transport in disordered organic photoconductors a Monte Carlo simulation study," *Phys. Status Solidi (b)* **175**(1), 15–56 (1993).
- ⁵⁷A. Janotti and C. G. V. de Walle, "Oxygen vacancies in ZnO," *Appl. Phys. Lett.* **87**(12), 122102 (2005).
- ⁵⁸V. Ischenko, S. Polarz, D. Grote, V. Stavarache, K. Fink, and M. Driess, "Zinc oxide nanoparticles with defects," *Adv. Funct. Mater.* **15**(12), 1945–1954 (2005).
- ⁵⁹K. Ide, K. Nomura, H. Hosono, and T. Kamiya, "Electronic defects in amorphous oxide semiconductors: A review," *Phys. Status Solidi (a)* **216**(5), 1800372 (2019).
- ⁶⁰C. Cho and N. C. Greenham, "Computational study of dipole radiation in re-absorbing perovskite semiconductors for optoelectronics," *Adv. Sci.* **8**(4), 2003559 (2021).
- ⁶¹C. Cho, B. Zhao, G. D. Tainter, J.-Y. Lee, R. H. Friend, D. Di, F. Deschler, and N. C. Greenham, "The role of photon recycling in perovskite light-emitting diodes," *Nat. Commun.* **11**(1), 611 (2020).
- ⁶²A. R. Bowman, M. Anaya, N. C. Greenham, and S. D. Stranks, "Quantifying photon recycling in solar cells and light-emitting diodes: Absorption and emission are always key," *Phys. Rev. Lett.* **125**(6), 067401 (2020).
- ⁶³Y. Guo, Y. Jia, N. Li, M. Chen, S. Hu, C. Liu, and N. Zhao, "Degradation mechanism of perovskite light-emitting diodes: An in situ investigation via electroabsorption spectroscopy and device modelling," *Adv. Funct. Mater.* **30**(19), 1910464 (2020).